Journal of Chromatography A, 1228 (2012) 270–275

Contents lists available at ScienceDirect

Journal of Chromatography A

journal homepage: www.elsevier.com/locate/chroma

Comparison of the gradient kinetic performance of silica monolithic capillary columns with columns packed with 3 μm porous and 2.7 μm fused-core silica particles

Axel Vaast[a], Ken Broeckhoven[a], Sebastiaan Dolman[b], Gert Desmet[a], Sebastiaan Eeltink[a,*]

[a] Vrije Universiteit Brussel, Department of Chemical Engineering, Pleinlaan 2, B-1050 Brussels, Belgium
[b] Bruker Biosciences, 1/28A Albert Street, Preston, VIC 3072, Melbourne, Australia

ARTICLE INFO

Article history:
Available online 4 August 2011

Keywords:
Column comparison
Kinetic plot
Poppe plot
Peptide mapping
Proteomics

ABSTRACT

The kinetic-performance limits of a capillary silica C18 monolithic column and packed capillary columns with fully-porous 3 μm and fused-core 2.7 μm silica C18 particles (all 5 cm long) were determined in gradient-elution mode for the separation of peptides. To establish a kinetic plot in gradient-elution mode, the gradient time to column dead time ratio (t_G/t_0) was maintained constant when applying different flow rates. The normalized gradient approach was validated by dimensionless chromatograms, obtained at different flow rates and gradient times by plotting them as a function of the retention factor. The separation performance of the different column types was visualized via kinetic plots depicting the gradient time required to achieve a certain peak capacity when operating at a maximum system pressure of 350 bar. The gradient steepness (applying t_G/t_0 = 10, 20, and 40) did not significantly affect the gradient performance limits for low (<250) peak-capacity separations. For high peak-capacity separations the peak capacity per unit time increases when increasing the t_G/t_0 ratio. The C-term contribution of the porous 3 μm and fused-core 2.7 μm was comparable yielding the same gradient kinetic-performance limits for fast separations at a column temperature of 60 °C. The capillary silica monolithic column showed the lowest contribution in mass transfer and permeability was higher than the packed columns. Hence, the silica monolith showed the best kinetic performance for both fast and high peak-capacity gradient separations.

1. Introduction

Over the last decades, HPLC has witnessed numerous developments in chromatographic column materials and instrumentation to yield a better compromise between the separation performance and analysis time. Large 10–30 μm irregular-shaped particle-packed columns have been replaced by columns packed with spherical particles, as small as sub-2-μm, with narrow particle-size distributions [1–3]. This led also to the development of ultra-high-pressure instrumentation needed to handle these new column types since column pressure increases inversely to the square of the particle size. To reduce the contribution of mass transfer (C term in the van Deemter equation) in the particles even further, fused-core particle technology has been re-introduced [4,5]. The exceptionally low plate-height values observed in conventional-bore HPLC columns for these particles have been attributed to a combined effect of a reduced C-term, a reduced Eddy-dispersion (A term) assumed to result from a very narrow particle-size distribution and a reduced longitudinal diffusion (B-term) contribution [6].

Monolithic columns, as an alternative stationary phase to packed columns, were introduced in the 1990s. A monolith is composed of a continuous macroporous (interconnected) support structure and is typically prepared from organic polymers [7,8] or silica precursors [9–11]. In particular, the simplicity of in situ preparation from liquid precursors in capillary column formats [12,13] and the excellent robustness of the columns [14] due the covalent attachment of the monolith to the wall are considered as major advantages compared to packed (capillary) columns. From the perspective of kinetic performance, monolithic materials can also be attractive since the flow-through pores, the size of the skeletons, and the total porosity can be fine-tuned by optimizing the composition of the polymerization mixture and the polymerization conditions [15–17].

Most comparisons of the separation performance are based on the van Deemter curves [18–21]. Gritti et al. compared 4.6 mm I.D. columns packed with 2.7 μm fused-core particles and columns packed with porous 3 μm particles for low-molecular weight

* Corresponding author. Tel.: +32 02 629 3324; fax: +32 02 629 3248.
E-mail address: seeltink@vub.ac.be (S. Eeltink).

0021-9673/$ – see front matter © 2011 Elsevier B.V. All rights reserved.
doi:10.1016/j.chroma.2011.07.089

test analytes and peptides. They found a 20% reduction in Eddy-dispersion contribution due to a narrow particle-size distribution and a 25% lower B contribution due to the solid core in the particle. No difference in C contribution was observed for low molecular-weight compounds whereas the C-term contribution of the Halo column was about a factor of two lower than that of a column packed with totally porous silica particles for compounds with low diffusivities [19]. Zheng et al. compared the performance of a 4.6 mm I.D. Chromolith silica monolithic columns with microparticulate columns packed with porous 3 μm ACE particles and 2.7 μm fused-core Halo particles for beta-methasone-17-valerate, which is an active pharmaceutical ingredient (MW = 476 Da) [19]. The minimum plate-heights values were determined at 10.2, 6.4 and 5.0 μm, respectively at a retention factor of around 8.5. The slope of the C-term region of the van Deemter curve was similar for the ACE and the Chromolith columns, whereas the C-term contribution of the Halo column was lower.

To assess the separation performance of columns with different morphologies the classical van Deemter curve does not longer suffice, since it does not incorporate the effect of column permeability on kinetic performance, which is one of the key drivers for the development of new (monolithic) support systems [22]. As an alternative for the van Deemter curve, Giddings proposed a graph depicting the analysis time versus (isocratic) plate number (N) values to compare the performance of high-performance LC (HPLC) with that of gas chromatography when operating columns at the maximum available operating pressure [23]. This approach has been extended to a family of kinetic plots [24,25] that can be used to compare the time required to obtain a specific number of plates for columns with different support formats and entail a variety of different representations including t_0 versus N, t_0/N versus N (Poppe plot [26]), t_0/N^2 versus N, etc.

The van Deemter curve and kinetic plots typically constitute plate-height values experimentally determined in isocratic liquid-chromatographic mode, while many applications, including proteomics peptide-mapping experiments, are performed in gradient mode. In 2006, Schoenmakers et al. [27] proposed the use of kinetic plots for peak-capacity production in gradient-elution liquid chromatography. This approach was validated by Zhang et al. [28], who conducted an experimental study in gradient-elution mode and compared the performance of a HALO C18 column with that of BEH C18, while keeping the gradient steepness constant. A theoretical framework and validation to construct kinetic plots from experimental data obtained in gradient mode was demonstrated by Broeckhoven et al. [29]. An important prerequisite of this approach is that analytes maintain the same retention behavior when operating the column at different flow rates. This implies that during data collection the gradient time (t_G) must be increased inversely proportionally to the flow rate (constant t_G/t_0) and thus when using longer columns the t_G must be compensated for the increase in t_0. To get a maximally representative measurement of the column performance under gradient conditions, it is also preferable that gradient conditions are selected such that the components elute over a sufficiently broad range of retention factors. The gradient conditions needed to achieve this might be different from support type to support type, because of differences in retention behavior. In addition, a correction for the effect of the system dwell volume is required when comparing columns with different lengths or I.D.

Especially in the field of proteomics research fast and efficient separation methods are required to analyze very small amounts of sample [30]. As a result, there is a strong interest in miniaturization of liquid-chromatography columns. The performance of capillary columns has frequently been tested in isocratic mode using low molecular weight analytes [31,32]. However, to the best of our knowledge, the gradient performance for the separation of biomolecules has not yet been established and visualized using gradient kinetic plots. In the present study the separation performance of different commercially-available capillary column supports, *i.e.* capillary columns packed with 3 μm porous and 2.7 μm fused-core silica particles, and a silica monolithic capillary column, is compared in gradient mode for peptide separations. The separation performance is visualized via gradient kinetic plots depicting the analysis time required to achieve a certain peak capacity when operating at maximum system pressure. System parameters (external band broadening and dwell volume) influencing the gradient performance is discussed. In addition, the effect of retention factor on gradient performance is demonstrated by applying different gradient steepness.

2. Materials and methods

2.1. Chemicals and materials

Acetonitrile (ACN, HPLC supra-gradient quality) and formic acid (FA, ≥99%) were purchased from Biosolve B.V. (Valkenswaard, The Netherlands). Uracil (99%, HPCE) and acetone were acquired from Sigma–Aldrich (Steinheim, Germany). A tryptic digest of bovine cytochrome *c* (1.6 nmol, Lyophilized) was purchased from Dionex Benelux (Amsterdam, The Netherlands). Deionized water (≤0.055 μS) was produced in-house using a Milli-Q gradient (Millipore, Molsheim, France) water purification system.

An ACE3C_{18} packed column (50 mm × 0.1 mm, 3 μm) from Advanced Chromatography Technology (Aberdeen, UK), a HALO fused-core C_{18} packed column (50 mm × 0.1 mm, total particle diameter is 2.7 μm with a 0.5 μm porous layer) from Advanced Materials Technologies (Wilmington, DE, USA), and a MonoCap C_{18} Nano-flow silica monolithic column (50 mm × 0.1 mm) from GL Sciences Inc. (Tokyo, Japan) were evaluated.

2.2. Instrumentation and LC conditions

HPLC experiments were performed on a Ultimate 3000 capillary LC system (Dionex Corporation, Germering, Germany) composed of a membrane degasser, a dual-ternary gradient pump, a well-plate sampler, column oven, and UV detector equipped with a 3 nL Z-shaped detector flow cell. Gradient separations were performed with the column placed in the oven at 60 °C, connected to the injector with 500 mm × 0.02 mm I.D. connection tubing and directly coupled to the 0.02 mm I.D. tubing of the 3 nL UV z-cell. Mobile-phase A was 0.05% FA in water, mobile phase B was 0.04% FA in 80:20% (v/v) ACN:H_2O. UV detection was performed at 210 nm at 20 Hz data collection rate and 0.05 s response time.

The column dead time (t_0) was determined by injection and detection of uracil (0.0015 mg/mL with 0.1 μL injections) at different flow rates. t_0 and retention times (t_R) were corrected for the residence time in the connections capillaries between the injector and the column and between the column and UV detector. The delay time (t_{delay}) was determined applying a gradient while adding 0.3% acetone in the mobile phase B. For the column pressure, the highest value encountered during the gradient run was taken, corresponding to the mobile-phase composition having the highest average viscosity.

Kinetic-plot measurements were performed using a tryptic cytochrome *c* digest (Dionex Benelux, Amsterdam, The Netherlands) applying 'delayed injections' using user-defined programs. On the column packed with 3 μm porous particles 0.25 pmol/μL cytochrome *c* digest, dissolved in mobile-phase A, was injected. The concentration was reduced to 0.125 pmol/μL for the fused-core column and the silica monolithic column to scale the injected amount to surface area.

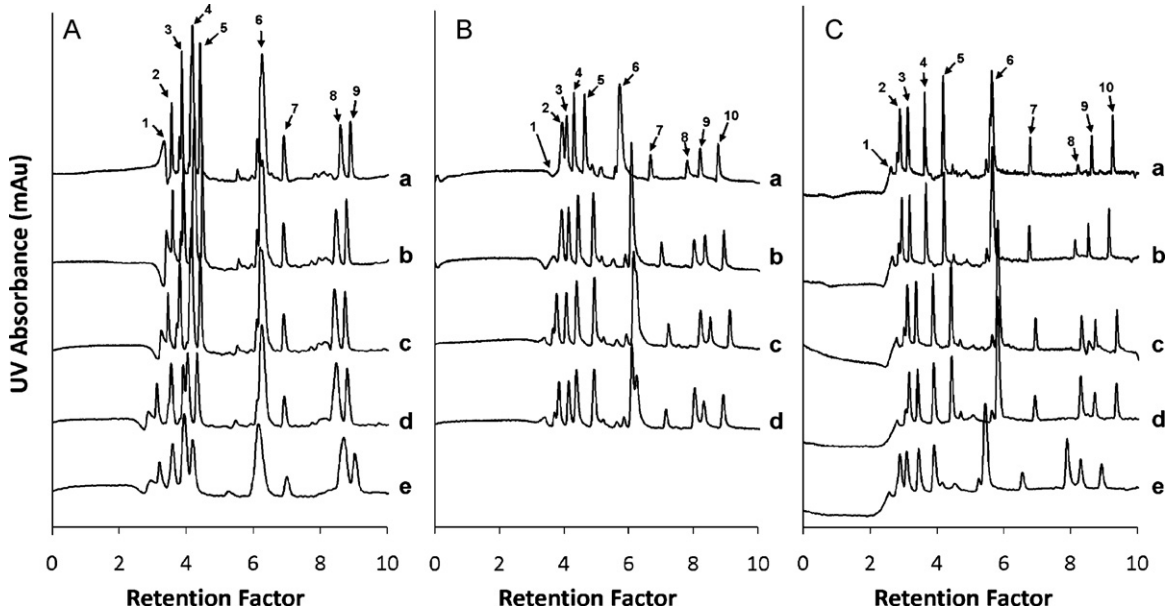

Fig. 1. Dimensionless chromatograms of a cytochrome *c* tryptic digest normalized to gradient retention factor for the capillary column (50 mm × 0.1 mm) packed with porous 3 μm particles (A), 2.7 μm fused-core particles (B), and the capillary silica monolithic column (C). The flow rates applied are 0.25 (a), 0.5 (b), 1.0 (c), 2.0 (d), and 4.0 μL/min (e). Due to lower permeability of the fused-core column the performance a 4 μL/min could not be determined. Gradient times were scaled to t_0 time be maintaining $t_G/t_0 = 10$. See Table 1 for other experimental conditions. Chromatograms are blank subtracted and times are corrected for elution times in connection capillaries.

3. Results and discussion

3.1. Dimensionless chromatograms

A tryptic cytochrome *c* digest was selected to represent a 'proteomics sample' since this sample mixture contains both hydrophilic (early eluting) and hydrophobic (late eluting) peptides and can be detected with UV detection. The start and final gradient composition were selected such that the first peptide eluted close at the start and the last peptide eluted close to the end of the gradient, so as to maximally cover all possible elution conditions. Due to the differences in surface area and chemistry between column types this approach may lead to a comparison where Δc is not the same. To avoid that the use of different gradient ranges would give any advantage to a specific column type, the performance of the columns was also characterized at different gradient steepness.

To maintain the same retention behavior when the column is operated at different flow rates [29], the t_G/t_0 ratio was maintained constant for each different investigated flow rate. t_0 was determined with uracil, which has the same residence time as the mobile phase. t_G was adjusted to maintain the t_G/t_0 ratio at 10, 20, and 40. Next, t_G was decreased inversely proportional to the increase in flow rate. Fig. 1A shows dimensionless chromatograms obtained on the column packed with porous 3 μm particles for a t_G/t_0 ratio of 10. Since the *x*-axis is normalized, by plotting them as a function of the retention factor instead of as a function of the absolute time, the chromatograms obtained at different flow rates are expected to coincide. The retention factor depicted at the *x*-axis corresponds to the average gradient retention factor ($k_G = t_R/t_0 - 1$). Some of the peaks contain multiple co-eluting peptides that are only resolved when the gradient time is increased. The peptides are well distributed over the elution window with retention factors ranging from 3.2 to 8.9. Some deviation in the observed retention factor window is explained by experimental variation in t_0 and $t_{0,external}$ measurements (although typically <3 s) and a decreased accuracy in gradient proportioning at low flow rates. The dimensionless chromatograms obtained on the fused-core column and the silica monolith, obtained for the same t_G/t_0 ratio of 10, are depicted in Fig. 1B and C, respectively. As can be noted the retention factor range for the different column types was approximately the same after adjusting the gradient span. The silica-monolithic capillary column clearly shows the best resolution between the peptides. Peptide 10 was not detected on the ACE column, and may stick to the surface. The peak area of peptide 8 in Fig. 1C decreases when applying lower flow rate. This may be due to proteolytic activity and the prolonged residence time of the peptides in the column at lower flow rates. Table 1 summarizes the column properties and experimental conditions applied.

It is important to note that the gradient delay volume (V_{delay} = 4.1 μL) of capillary LC systems is relatively large with respect to the column volume. This strongly affected the retention factors and peak widths of the hydrophilic peptides. At the gradient start conditions (even at 0% ACN) the hydrophilic peptides are not retained and elute at isocratic conditions during the delay time, resulting in broad peaks. Hydrophobic peptides that elute at higher solvent strength are not influenced in peak width due to the so-called 'on–off mechanism'. To prevent isocratic elution during the dwell time, the kinetic-plot measurements were performed using 'delayed injections' to ensure that both sample and gradient slope reach the front of the column at the same time. In addition, the extra-column volume between injector and column was minimized as much as possible to reduce extra-column dispersion effects.

3.2. Gradient kinetic plots

For construction of kinetic plots, the peak widths (W), retention times (t_R), and column pressure (ΔP) were experimentally deter-

Table 1
Gradient span and corresponding retention factor range determined for each column type at t_G/t_0 = 10, 20, and 40.

	3 μm (porous)	2.7 μm (fused core)	silica monolith
Gradient span (%ACN)	4–48.0	0–44.8	0–33.2
k range (t_G/t_0 = 10)	3.2–8.9	3.4–8.6	2.9–8.7
k range (t_G/t_0 = 20)	3.9–14.5	3.2–13.0	2.8–14.7
k range (t_G/t_0 = 40)	4.6–24.8	4.6–22.9	3.9–25.6

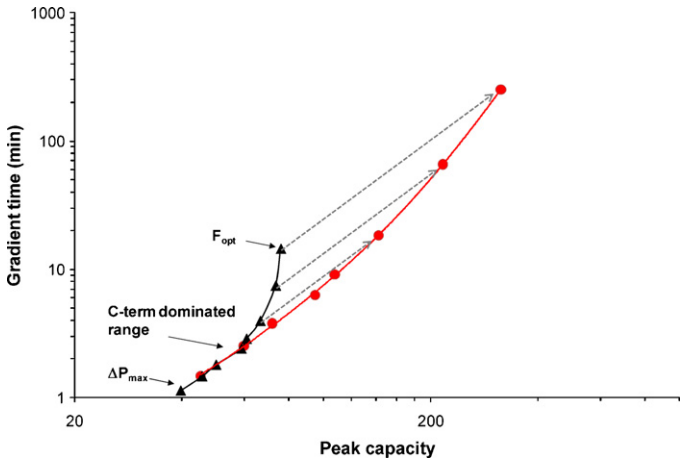

Fig. 2. Construction of a gradient kinetic plot. Experimental n_c and t_R data (▲) measured on a 50 mm column packed with 3 μm porous silica particles (fixed-length kinetic plot). Kinetic performance limit (●) extrapolated for a maximum system pressure of 350 bar at $t_G/t_0 = 10$ by increasing the column length and maintaining the same mobile-phase velocity (free-length kinetic plot).

mined from chromatograms. The variation in run-to-run W, t_R, and ΔP was smaller than 0.1%, 2.2% and 0.1%, respectively ($n = 6$). The peak capacity (n_c) was determined applying Eq. (1).

$$n_c = \frac{t_G}{W} + 1 \tag{1}$$

Fig. 2 shows the experimental n_c and gradient time (t_G) data for a peptide eluting at $k = 6.8$ measured on a 50 mm long column packed with 3 μm porous silica particles varying the flow rate between 0.0625 μL/min and 4 μL/min and maintaining the t_G/t_0 ratio at 10. Most of the experimental data points in this fixed-length kinetic plot were obtained in the C-term region of the Van Deemter curve and the optimal mobile-phase velocity was observed close to the lowest applied flow rate ($F_{opt} \sim 0.125$ μL/min yielding a column pressure of approximately 5 bar). This representation, shows that the highest peak capacity is achieved when operating a column at the optimum linear velocity, while higher flow rates (*i.e.* operating in the C-term domain) can be employed for less demanding separations with greater speed. Free-length gradient-kinetic plots were subsequently established from the experimental $n_{c,exp}$ and $t_{G,exp}$ data obtained on a given column length via extrapolation of the data using a length-elongation factor λ using Eqs. (2)–(4):

$$\lambda = \frac{\Delta P_{max}}{\Delta P_{exp}} \tag{2}$$

$$n_{c,max} = 1 + (n_{c,exp} - 1)\sqrt{\lambda} \tag{3}$$

$$t_{G,max} = \lambda t_{G,exp} \tag{4}$$

where ΔP_{max} is the maximum system pressure and ΔP_{exp} the experimental column pressure recorded (corrected for the pressure contribution from connections tubing from injector to column and from column to the detector cell). The resulting values depict the kinetic-performance limit, *i.e.* the highest peak capacity that can be generated in the shortest possible gradient time, on columns packed with porous 3 μm particles at $\Delta P_{max} = 350$ bar and $t_G/t_0 = 10$. When the requirements on the peak capacities are not severe, high mobile-phase velocities can be used, with plate heights in the C-dominated region, and the required gradient time becomes directly proportional to the peak capacity.

The variation in gradient kinetic-performance limits as measured for the different peptides in the mixture is demonstrated

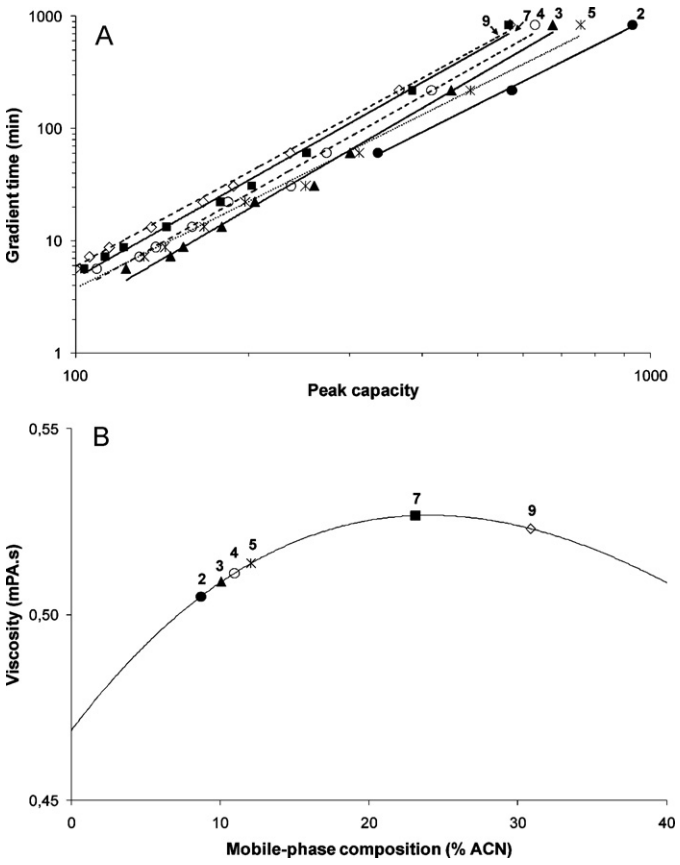

Fig. 3. Variation in gradient kinetic-performance limits for different peptides that elute within the gradient window on a capillary column packed with porous 3 μm particles (A) and effect of the mobile-phase composition determined at the point of elution on viscosity (B). The numbers correspond to the peptides eluting in Fig. 1 obtained at $t_G/t_0 = 20$, other experiential conditions similar as Fig. 1. Solid symbols (and trendlines) depict peptides of the same molecular weight (MW ranging between 633 and 778 Da). Open circle and cross depict high molecular-weight peptides (MW of 1583 and 2008 Da).

in Fig. 3A. The represented data are for a gradient with $t_G/t_0 = 20$. Similar plots were obtained for the two other considered gradient conditions. For the peptide eluting at $k = 4.2$ (Peptide 2) only the data points close to the van Deemter optimum are shown, since the peptide co-eluted at higher flow rates and the peak width could not be determined.

Reporting the peak capacity based on total gradient time, the observed variation in kinetic performance is directly related to the differences in peak width of the different peptides. For example, at a flow rate of 1 μL/min the variation in W between the different peptides was ranging from 0.034 and 0.063 min, thus explaining the shift among the different curves in Fig. 3A. The peak width W in gradient elution is given by

$$W = 4\frac{\sqrt{N}}{t_0}(1 + k_e) = 4\frac{\sqrt{L/H}}{t_0}(1 + k_e) \tag{5}$$

where k_e is the retention factor of the compound at the point of elution, L the column length, and H the plate height. As a result, peak width in gradient-elution mode is determined by its retention properties (influencing k_e) and by H. Similar as in isocratic elution, H is affected by the Eddy-diffusion (A-term), longitudinal-diffusion (B-term), and mass-transfer (C-term) contributions. Generally, a small increase in the peak width is observed with increasing retention factor. The variation in peak width may partly be explained by the difference in diffusion coefficients originating from the mobile-phase viscosity history experienced and the molecular weight of

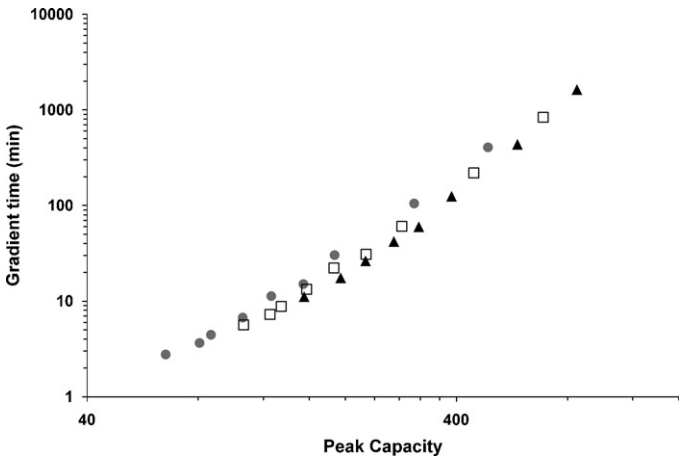

Fig. 4. Effect of gradient steepness on peak capacity and time at $t_G/t_0 = 10$ (●), $t_G/t_0 = 20$ (□), and $t_G/t_0 = 40$ (▲) on a capillary column packed with porous 3 μm particles.

the peptides. Fig. 3B shows the effect of mobile-phase composition on viscosity at 60 °C and a column pressure of 350 bar [33]. The data points represent the different peptides corresponding to Fig. 1 of which the mobile-phase composition was determined at their moment of elution. Peptides 2, 3, and 7 (solid symbols and lines) have approximately the same molecular weight (MW ranges between 633 and 778 Da) but experience a different mobile-phase viscosity history. As a result, the diffusion coefficient of early-eluting peptides is slightly higher, yielding smaller peak widths (operating in the C-term region) and consequently higher peak capacities. Although the molecular weight of peptide 4 is larger (1583 Da) than that of peptide 7, it experiences a slightly lower average mobile-phase viscosity and consequently yields a higher peak capacity. The low peak capacity (broader peak width) of peptide 9 may be related to the large molecular weight (2008 Da), the higher experienced average viscosity (see Fig. 3B) and correspondingly its lower diffusion coefficient. The variations in peak width observed for the different peptides on the silica monolith and fused-core columns were smaller. This may partly be explained by the reduced surface area and porous zone of the silica monolith and the fused-core column. Due to reduced diffusion distance the effect of slightly different diffusion coefficient on C-term contribution may be reduced. For the construction of all further kinetic plots in the manuscript the sample averaged peak capacity was used.

Fig. 4 shows free-length gradient kinetic plots based on the average peak width obtained on the column packed with porous 3 μm silica particles at $t_G/t_0 = 10$, 20, and 40. The corresponding retention factor ranges are 3.2–8.9, 3.9–14.5, and 4.6–24.8 respectively. The gradient steepness (applying $t_G/t_0 = 10$, 20, and 40) did not significantly affect the gradient performance limits for fast separations with peak capacities below approximately 250. For high peak-capacity separations the peak capacity per unit time increases when increasing the t_G/t_0 ratio. No peak-compression effects were observed when applying short gradients. The gradient kinetic plots of the fused-core and of the silica-monolithic columns measured at different t_G/t_0 ratios showed the same trend (data shown in Supplementary Information S1). Although the mobile-phase composition at the moment of elution decreases with approximately 4% with increasing t_G/t_0 ratio, this has only marginal effect on the C-term contribution since the data points are positioned at the top of the viscosity curve depicted in Fig. 3B. As a consequence, no significant differences in peak width were expected between the different considered t_G/t_0 ratios, as was indeed observed for the fused-core and the silica-monolithic columns.

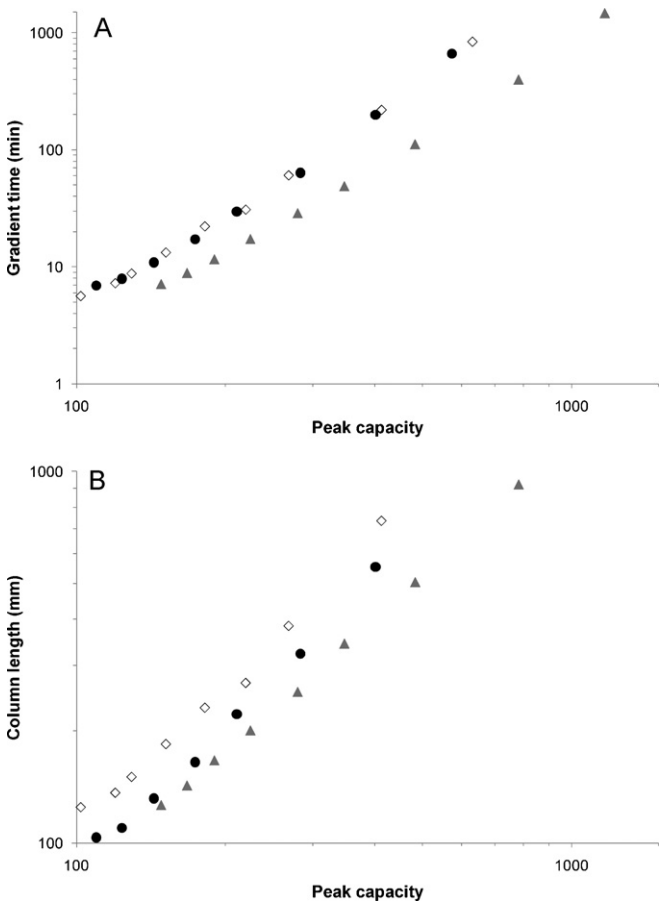

Fig. 5. Gradient kinetic-performance limits (A) and corresponding column lengths (B) of capillary columns packed with 3 μm porous (◊) and 2.7 μm fused-core particles (●) and the capillary silica monolith (▲) operating at $t_G/t_0 = 20$.

3.3. Column comparison

The comparison of the gradient performance of the different column types at $t_G/t_0 = 20$ is shown in Fig. 5. The kinetic-performance limits ($n_{c,max}$ versus $t_{G,max}$) are depicted in Fig. 5A, the corresponding required column lengths are shown in Fig. 5B. Despite the smaller particle size and the presences of the solid core reducing the B- and the C-term contributions to band broadening, the gradient performance of the superficially porous particles is equal to that of the fully porous 3 μm packed column. However, the required column length of the fused-core columns is smaller. The maximum peak capacity that can be generated on the silica monolith was significantly higher than that on both microparticulate columns. For example, when applying a 30 min gradient, the peak capacity is 280 on the long silica monolith versus 220 on the packed columns. This is partly because of the clearly smaller peak widths that can be generated compared to the microparticulate columns (see Fig. 1, where the average peak width for the silica monolithic column was significantly smaller at all flow rates compared to that of the fused core column and column packed with porous particles) and partly because of the higher permeability of the silica monolith containing relatively large flow-through pores compared to the interstitial pores between packed beds (40% higher permeability than the fused-core column). Also, for fast separations the silica monolith outperformed the packed columns. For example, to generate a peak capacity of 150 the separation using a silica monolith is completed within the 7 min gradient, whereas the required gradient duration is 12 min using a packed column.

When comparing the gradient kinetic-performance limits of peptides with that of small molecules on 4.6 mm I.D. columns (packed with the same type of stationary phase) [29] it can be noted that, although maximum system pressure of the system used in this study was lower, the maximum peak capacity that can be generated is significantly higher. This is because the optimal linear velocity is directly proportional to the diffusion coefficient of the compound, which depends directly on its molecular weight. These results are in line with recent studies showing that molecular weight of the model compound could strongly impact the kinetic plot performance limits [31,34].

4. Conclusions

In this study the gradient performance of 5 cm capillary columns packed with porous 3 μm and 2.7 μm fused-core particles and a silica monolithic column was evaluated using the kinetic-plot method. The method takes the effect of column structure on peak width and permeability into account. The performance of the silica monolith was superior to both microparticulate columns (packed with 3 μm porous and 2.7 μm fused-core particles). This is mainly due to their better band-broadening characteristics and the higher permeability. It is important to note the performance limits depicted in the gradient kinetic plot assumes that columns of different length can be produced equally well. This aspect was not validated in the present study and also only one column of each type was tested. However, different regions of the kinetic plot become accessible using zero-dead-volume column-coupling devices developed for capillary columns. We are planning to use this gradient-kinetic plot approach to optimize the separation conditions for columns that differ in length and for the characterization of different column types when separating small and large molecules in gradient-elution mode.

Acknowledgments

Support of this work by a grant of the Research Foundation Flanders (G.0919.09) is gratefully acknowledged. K.B. acknowledges a post-doc research grant from the Research Foundation – Flanders (FWO Vlaanderen). The authors would like to thank M. Kurano of ATAS GL International Eindhoven, The Netherlands) for donation of the silica monolithic capillary columns.

Appendix A. Supplementary data

Supplementary data associated with this article can be found, in the online version, at doi:10.1016/j.chroma.2011.07.089.

References

[1] K.D. Patel, A.D. Jerkovich, J.C. Link, J.W. Jorgenson, Anal. Chem. 76 (2004) 5777.
[2] J.S. Mellors, J.W. Jorgenson, Anal. Chem. 76 (2004) 5441.
[3] E. Olàh, S. Fekete, J. Fekete, K. Ganzler, J. Chromatogr. A 1217 (2010) 3642.
[4] J.J. Kirkland, Anal. Chem. 64 (1992) 1239.
[5] J.J. Kirkland, F.A. Truszkowski, C.H. Dilks Jr., G.S. Engel, J. Chromatogr. A 890 (2000) 3.
[6] D. Cabooter, A. Fanigliulo, G. Bellazzi, B. Allieri, A. Rottigni, G. Desmet, J. Chromatogr. A 1217 (2010) 7074.
[7] F. Svec, J.M.J. Fréchet, Anal. Chem. 64 (1992) 820.
[8] F. Svec, J.M.J. Fréchet, Science 273 (1996) 205.
[9] H. Minakuchi, K. Nakanishi, N. Soga, N. Ishizuka, N. Tanaka, Anal. Chem. 68 (1996) 3498.
[10] N. Tanaka, H. Kobayashi, N. Ishizuka, H. Minakuchi, K. Nakanishi, K. Hosoya, T. Ikegami, J. Chromatogr. A 965 (2002) 35.
[11] N. Tanaka, H. Kobayashi, K. Nakanishi, H. Minakuchi, N. Ishizuka, Anal. Chem. 73 (2001) 420A.
[12] S. Eeltink, S. Dolman, F. Detobel, R. Swart, M. Ursem, P.J. Schoenmakers, J. Chromatogr. A 1217 (2010) 6610.
[13] T.B. Stachowiak, T. Rohr, E.F. Hilder, D.S. Peterson, M. Yi, F. Svec, J.M.J. Fréchet, Electrophoresis 24 (2003) 3689.
[14] J. Courtois, M. Szumski, E. Byström, A. Iwasiewicz, A. Shchukarev, K. Irgum, J. Sep. Sci. 29 (2006) 14.
[15] K. Nakanishi, N. Tanaka, Acc. Chem. Res. 40 (2007) 863.
[16] T. Hara, H. Kobayashi, T. Ikegami, K. Nakanishi, N. Tanaka, Anal. Chem. 78 (2006) 7632.
[17] S. Eeltink, J.M. Herrero-Martinez, G.P. Rozing, P.J. Schoenmakers, W.T. Kok, Anal. Chem. 77 (2005) 7342.
[18] F. Gritti, A. Cavazzini, N. Marchetti, G. Guiochon, J. Chromatogr. A 1157 (2007) 289.
[19] J. Zheng, D. Patel, Q. Tang, R.J. Markovich, A.M. Rustum, J. Pharm. Biomed. Anal. 50 (2009) 815.
[20] A. Abrahim, M. Al-Sayah, P. Skrdla, Y. Bereznitski, Y. Chen, N. Wu, J. Pharm. Biomed. Anal. 51 (2010) 131.
[21] F. Gritti, I. Leonardis, D. Shock, P. Stevenson, A. Shalliker, G. Guiochon, J. Chromatogr. A 1217 (2010) 1589.
[22] S. Eeltink, P. Gzil, W.T. Kok, P.J. Schoenmakers, G. Desmet, J. Chromatogr. A 1130 (2006) 108.
[23] J.C. Giddings, J. Chromatogr. 18 (1965) 221.
[24] G. Desmet, D. Clicq, P. Gzil, Anal. Chem. 77 (2005) 4058.
[25] S. Eeltink, W.M.C. Decrop, F. Steiner, M. Ursem, D. Cabooter, G. Desmet, W.T. Kok, J. Sep. Sci. 33 (2010) 2629.
[26] H. Poppe, J. Chromatogr. A 778 (1997) 3.
[27] X. Wang, D.R. Stoll, P.W. Carr, P.J. Schoenmakers, J. Chromatogr. A 1125 (2006) 177.
[28] Y. Zhang, X. Wang, P. Mukherjee, P. Petersson, J. Chromatogr. A 1216 (2009) 4597.
[29] K. Broeckhoven, D. Cabooter, F. Lynen, P. Sandra, G. Desmet, J. Chromatogr. A 1217 (2010) 2787.
[30] A.R. Ivanov, L. Zang, B.L. Karger, Anal. Chem. 75 (2003) 5306.
[31] S. Fekete, J. Fekete, K. Ganzler, J. Pharm. Biomed. Anal. 49 (2009) 64.
[32] S. Eeltink, G. Desmet, G. Vivó-Truyols, G.P. Rozing, P.J. Schoenmakers, W.T. Kok, J. Chromatogr. A 1104 (2006) 256.
[33] J. Billen, K. Broeckhoven, A. Liekens, K. Choikhet, G. Rozing, G. Desmet, J. Chromatogr. A 1210 (2008) 30.
[34] J. Ruta, D. Guillarme, S. Rudaz, J.-L. Veuthey, J. Sep. Sci. 33 (2010) 2465.